Generalized Approximate Message Passing Equalization for Multi-Carrier Faster-Than-Nyquist Signaling

Yunsi Ma, *Student Member, IEEE,* Nan Wu, *Member, IEEE,* J. Andrew Zhang, *Senior Member, IEEE*
Bin Li, *Member, IEEE,* and Lajos Hanzo, *Fellow, IEEE*

***Abstract*—Multi-carrier faster-than-Nyquist (MFTN) signaling constitutes a promising spectrally efficient non-orthogonal physical layer waveform. In this correspondence, we propose a pair of low-complexity generalized approximate message passing (GAMP)-based frequency-domain equalization (FDE) algorithms for MFTN systems operating in multipath channels. To mitigate the ill-condition of the resultant equivalent channel matrix, we construct block circulant interference matrices by inserting a few cyclic postfixes, followed by truncating the duration of the inherent two-dimensional interferences. Based on the decomposition of the block circulant matrices, we develop a novel frequency-domain received signal model using the two-dimensional fast Fourier transform for mitigating the colored noise imposed by the non-orthogonal matched filter. Moreover, we derive a GAMP-based FDE algorithm and its refined version, where the latter relies on approximations for circumventing the emergence of the ill-conditioned matrices. Our simulation results demonstrate that, for a fixed spectral efficiency, MFTN signaling can significantly improve the bit error rate (BER) performance by jointly optimizing the time- and frequency-domain packing factors. Compared to its Nyquist-signaling counterpart, our proposed MFTN systems employing the refined GAMP equalizer can achieve about 39% higher transmission rates at a negligible BER performance degradation.**

***Index Terms*—Multi-carrier faster-than-Nyquist signaling, frequency-domain equalization, generalized approximate message passing, block circulant matrix with circulant blocks.**

I. INTRODUCTION

Given the paucity of spectral resources, faster-than-Nyquist (FTN) signaling has attracted substantial attention as a benefit of its high capacity [1]–[4]. It constitutes a prominent member of the non-orthogonal multiple access (NOMA) family [5], [6] and it readily lends itself to amalgamation with multiple-input multiple-output (MIMO) [7] systems. To further increase its spectral efficiency (SE), multi-carrier FTN (MFTN) signaling was then proposed in [8]. By relaxing the constraints on the orthogonality of the signaling pulse and subcarriers with respect to the symbol interval and frequency spacing, MFTN signaling can provide a higher SE than one-dimensional FTN signaling. However, MFTN signaling inevitably inflicts severe intersymbol interferences (ISIs) and intercarrier interferences (ICIs), which result in a prohibitively high receiver complexity. Accordingly, conceiving low-complexity equalization is critical, but challenging for MFTN systems.

A popular class of MFTN signaling employs transmit precoding [9], [10]. Specifically in [9], a linear precoding scheme combined with receiver-side turbo ICI cancellation was developed for MFTN systems. To circumvent the potential transmission contamination caused by small eigenvalues of the interference matrix, a TomlinsonHarashima precoding (THP) method was designed for one-dimensional frequency packed MFTN systems using high-order modulation in [10].

The other class of techniques employs advanced equalization at the receiver [11]–[16]. In [11], the optimal maximum *a posteriori* (MAP) method was derived by harnessing the Bahl-Cocke-Jelinek-Raviv (BCJR) algorithm, which however imposed an exponentially escalating complexity. In [12], a suboptimal reduced-state BCJR detector based on successive interference cancellation (SIC) was proposed. However, its complexity still increases exponentially with the length of the truncated interferences. As a further advance, a memoryless turbo receiver having linearly increasing complexity was designed for MFTN systems in [13]. Hence, this less complex, but also less powerful receiver results in a bit error rate (BER) performance loss in aggressive time-frequency packing scenarios. To strike a BER performance versus complexity trade-off, a pair of minimum mean-squared error (MMSE)-based equalizers were developed for MFTN signaling in [14]. Unfortunately, the two-dimensional (2D) MMSE-based equalizer suffers from a significant performance loss in severe ICI scenarios. By contrast, the one-dimensional version of [14] combined with SIC can asymptotically approach the MAP performance. However, the complexity of both methods is still dominated by the associated matrix inversion calculations. For longhaul optical transmission scenarios, turbo parallel interference cancellation (PIC) schemes combined with BCJR-based ISI cancellation were proposed for time-frequency packed (TFP) wavelength-division-multiplexed (WDM) systems [15], [16]. These systems separately eliminate the inherent 2D interferences of MFTN signaling, but a joint 2D interference cancellation scheme is expected to achieve better performance.

Most of the above-mentioned equalizers were proposed for additive white Gaussian noise (AWGN) channels, and they cannot deal with the colored noise imposed by non-orthogonal matched filtering. It has been demonstrated that mitigating the effect of colored noise improves the BER performance [3]. Hence, it is necessary to tackle the inherent colored noise problem in order to design an efficient MFTN receiver. In [17],

This work is supported by the "National Science Foundation of China (NSFC)" (Grant Nos. 61971041, 62001027). L. Hanzo would like to acknowledge the financial support of the Engineering and Physical Sciences Research Council projects EP/P034284/1 and EP/P003990/1 (COALESCE) as well as of the European Research Council's Advanced Fellow Grant QuantCom (Grant No. 789028). *(Corresponding Author: Nan Wu.)*

Y. Ma, N. Wu and B. Li are with the School of Information and Electronics, Beijing Institute of Technology, Beijing 100081, China (e-mail: yunsi@bit.edu.cn; wunan@bit.edu.cn; binli@bit.edu.cn).

J. Andrew Zhang is with the Global Big Data Technologies Centre with the School of Electrical and Data Engineering, University of Technology Sydney, Sydney, NSW 2007, Australia (e-mail: andrew.zhang@uts.edu.au).

L. Hanzo is with the School of Electronics and Computer Science, University of Southampton, Southampton SO17 1BJ, U.K. (e-mail: lh@ecs.soton.ac.uk).

the authors proposed a Gaussian message passing (GMP)-based time-domain equalizer (TDE) relying on a vector-form trellis interference structure for MFTN systems operating in multipath channels. The truncated non-diagonal covariance matrix of the colored noise was exploited for improving the accuracy of message updating. To develop a parametric message passing receiver, the discrete *a priori* probabilities of the transmitted symbols are approximated by Gaussian distributions in [17], which results in an additional BER performance degradation. Moreover, MFTN signaling tends to suffer from a severe ill-conditioning problem, when the packing factors are significantly reduced, which may lead to the divergence of the equalization algorithms. However, there is a paucity of studies on tackling the ill-conditioning problem of MFTN signaling.

In this correspondence, we propose a pair of low-complexity equalization algorithms for MFTN systems operating in multipath channels. By inserting several cyclic postfixes and ignoring the insignificant interferences, we construct a block circulant interference matrix constituted by circulant blocks for reducing the condition number and mitigating the ill-conditioning problem of MFTN signaling. To diagonalize the covariance matrix of the colored noise, we reformulate the frequency-domain (FD) received signal model with the aid of the 2D fast Fourier transform (FFT). Building on this model, a parametric generalized approximated message passing (GAMP)-based FD equalization (FDE) algorithm is derived. To avoid the potential noise enhancement caused by the ill-conditioned matrices, we also design a refined GAMP-based FDE algorithm by invoking certain approximations. As a benefit, the complexity will only grow logarithmically with the number of transmitted symbols.

Notations: $\mathbf{0}_N$ and $\mathbf{1}_N$ represent all-zero and all-one column-vectors, respectively, while $\mathbf{0}_{N\times N}$ and $\mathbf{I}_N$ denote all-zero and identity matrices of size $N \times N$. Each element of the normalized discrete Fourier transform (DFT) matrix $\mathbf{F}_N$ is $F_{m,n} = N^{-1/2}\exp(-j2\pi(m-1)(n-1)/N)$. The operation $\mathcal{D}(\mathbf{x})$ or $\mathcal{D}(\mathbf{X})$ construct a diagonal matrix from the vector $\mathbf{x}$ or from the main diagonal vector of the square matrix $\mathbf{X}$. The operators $(\cdot)^T$ and $(\cdot)^H$ calculate the transpose and conjugate transpose of a matrix. The operators $\odot$, $\oslash$, $\otimes$, and $\propto$ denote element-wise product, element-wise division, Kronecker product, and equality up to a constant normalization factor. The notation $|\cdot|$ is used to compute the absolute value element-by-element. The complex Gaussian distribution of $\mathbf{x}$ with the mean vector $\mathbf{m}_\mathbf{x}$ and covariance matrix $\mathbf{V}_\mathbf{x}$ is expressed as $\mathcal{CN}(\mathbf{x};\mathbf{m}_\mathbf{x},\mathbf{V}_\mathbf{x})$. Moreover, $\mathbb{E}\{\cdot\}$ and $\mathbb{V}\{\cdot\}$ denote the calculations of expectation and variance.

II. System Model

We consider the universal FDE-based low-density parity-check (LDPC)-coded MFTN system of Fig. 1. The N_b input bits $\mathbf{b} = [b_0, \cdots, b_{N_\text{b}-1}]^T$ are encoded into N_c LDPC-coded bits $\mathbf{c} = [c_0, \cdots, c_{N_\text{c}-1}]^T$, which are then mapped onto an M-ary constellation to generate N_s modulated symbols $\mathbf{x} = [x_0, \cdots, x_{N_\text{s}-1}]^T$. Assume that the coded MFTN system contains K subcarriers and each subcarrier conveys $N = N_\text{s}/K$ symbols. Through a serial-to-parallel (S/P) converter, we obtain K parallel modulated symbol vectors $\mathbf{x}_0, \cdots, \mathbf{x}_{K-1}$ associated with $\mathbf{x}_k = [x_{k,0}, \cdots, x_{k,N-1}]^T, k = 0, \cdots, K-1$. Then, the first $2N_\text{p}$ modulated symbols of each subcarrier are concatenated to $\mathbf{x}_k$ as cyclic postfixes. The extended $\mathbf{x}_k$ is then passed through a pulse shaping filter $p(t)$. Each output sequence is then assigned to a subcarrier and the first $2K_\text{p}$ subcarriers are also inserted as cyclic postfixes in the FD. For MFTN signaling, we employ pulse shaping filters associated with the time interval τT and the overlapped subcarriers with frequency spacing of νF for improving the SE, where $\tau, \nu \in (0, 1]$ are the time and frequency packing factors, respectively, T is the Nyquist time interval, and F is the minimum orthogonal frequency spacing. Then non-orthogonal multi-carrier modulation can be efficiently carried out by inverse FFT (IFFT) modules [18]. After that, through a parallel-to-serial (P/S) converter, the baseband transmitted MFTN signal is expressed as

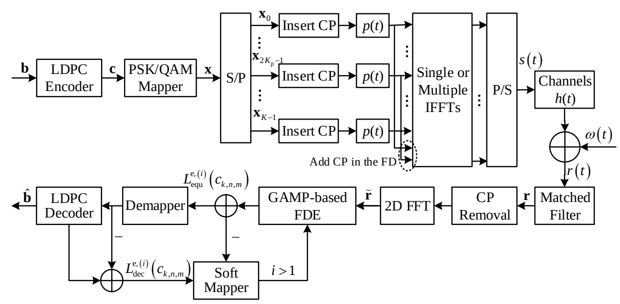

Fig. 1: FDE-based transceiver structure of MFTN signaling.

$$s(t) = \sum_{k=0}^{\bar{K}-1}\sum_{n=0}^{\bar{N}-1} x_{k,n}\, p(t - n\tau T) e^{j2\pi k\nu F t}, \tag{1}$$

where n and k are the time and subcarrier indexes, $\bar{K} = K + 2K_\text{p}$, and $\bar{N} = N + 2N_\text{p}$. In this correspondence, we employ a root-raised cosine (RRC) shaping pulse $p(t)$ with a roll-off factor β. For other non-orthogonal signaling schemes [19]–[21], the shaping pulse $p(t)$ can be adjusted and the following derivations are still valid.

After transmission over a multipath channel, the received MFTN signal is fed into a non-orthogonal matched filter, which yields

$$\begin{aligned} r_{k_\text{r},n_\text{r}} &= \sum_{l=0}^{L-1} h_l \int_{-\infty}^{\infty} s(t - l\tau T) p(t - n_\text{r}\tau T) e^{-j2\pi k_\text{r}\nu F t} dt + \omega_{k_\text{r},n_\text{r}} \\ &= \sum_{l=0}^{L-1} h_l \sum_{k_\text{t}=0}^{\bar{K}-1}\sum_{n_\text{t}=0}^{\bar{N}-1} x_{k_\text{t},n_\text{t}} e^{-j2\pi k_\text{t} l\nu F\tau T} \int_{-\infty}^{\infty} p(t - n_\text{r}\tau T) \\ &\qquad \times p(t - n_\text{t}\tau T - l\tau T) e^{j2\pi(k_\text{t}-k_\text{r})\nu F t} dt + \omega_{k_\text{r},n_\text{r}} \\ &= \sum_{l=0}^{L-1} h_l \sum_{k_\text{t}=0}^{\bar{K}-1}\sum_{n_\text{t}=0}^{\bar{N}-1} A_\text{p}(\varpi_\Delta \tau T, k_\Delta \nu F) \psi_{k_\Delta,n_\text{r}}^{k_\text{t},l} x_{k_\text{t},n_\text{t}} + \omega_{k_\text{r},n_\text{r}}, \end{aligned} \tag{2}$$

where h_l is the l-th channel coefficient, L is the channel's impulse-response duration, $A_\text{p}(\tau T, \nu F) = \int_{-\infty}^{+\infty} p(t)p(t -$

$\tau T)e^{j2\pi\nu Ft}dt$ is the ambiguity function, $\psi_{k_\Delta,n_\mathrm{r}}^{k_\mathrm{t},l} = \lambda_{k_\mathrm{t}}^{l}\theta_{k_\Delta}^{n_\mathrm{r}} = e^{-j2\pi k_\mathrm{t} l\nu F\tau T}e^{j2\pi k_\Delta n_\mathrm{r}\nu F\tau T}$, $\varpi_\Delta = n_\Delta + l$, $n_\Delta = n_\mathrm{t} - n_\mathrm{r}$ and $k_\Delta = k_\mathrm{t} - k_\mathrm{r}$ denote the intervals of symbols and subcarriers, $\omega_{k_\mathrm{r},n_\mathrm{r}} = \int_{-\infty}^{\infty} w(t)p(t - n_\mathrm{r}\tau T)e^{-j2\pi k_\mathrm{r}\nu Ft}dt$ and finally $w(t)$ is an AWGN process with zero mean and variance σ_0^2.

By removing the first and the last K_p subcarriers and N_p received samples of each subcarrier, we obtain the received vector $\mathbf{r} = [\mathbf{r}_{K_\mathrm{p}}^T, \cdots, \mathbf{r}_{K_\mathrm{p}+K-1}^T]^T$ with $\mathbf{r}_k = [r_{k,N_\mathrm{p}}, \cdots, r_{k,N_\mathrm{p}+N-1}]^T$. Since the ISIs and ICIs decay upon increasing the time interval and frequency spacing, we only consider the truncated interferences emanating from the adjacent N_I symbols and K_I subcarriers to reduce the computational complexity of the MFTN receivers. Assuming that N_p and K_p are more than N_I and K_I, respectively, the received MFTN signal can be approximately reformulated as

$$\mathbf{r} = \sum_{l=0}^{L-1} h_l \sum_{k_\Delta \in \mathcal{I}} \mathbf{\Theta}_{k_\Delta}\mathbf{\Xi}_{k_\Delta,l}\bar{\mathbf{\Lambda}}_l\mathbf{x} + \boldsymbol{\omega} = \mathbf{G}\mathbf{x} + \boldsymbol{\omega}, \tag{3}$$

where $\mathbf{G} = \sum_{l=0}^{L-1} h_l\mathbf{G}_l$ is the equivalent channel matrix with $\mathbf{G}_l = \sum_{k_\Delta\in\mathcal{I}} \mathbf{\Theta}_{k_\Delta}\mathbf{\Xi}_{k_\Delta,l}\bar{\mathbf{\Lambda}}_l$, $\mathcal{I} = \{-K_\mathrm{I}, -K_\mathrm{I}+1, \cdots, 0, \cdots, K_\mathrm{I}\}$, $\mathbf{\Theta}_{k_\Delta} = \mathbf{I}_K \otimes \mathcal{D}(\boldsymbol{\theta}_{k_\Delta})$ is an $N_\mathrm{s} \times N_\mathrm{s}$ diagonal matrix with $\boldsymbol{\theta}_{k_\Delta} = [\theta_{k_\Delta}^{N_\mathrm{p}}, \cdots, \theta_{k_\Delta}^{N_\mathrm{p}+N-1}]^T$, $\mathbf{\Xi}_{k_\Delta,l}$ is an $N_\mathrm{s} \times N_\mathrm{s}$ block circulant matrix with K^2 circulant blocks, $\bar{\mathbf{\Lambda}}_l = \mathcal{D}(\bar{\boldsymbol{\lambda}}_l) \otimes \mathbf{I}_N$ is an $N_\mathrm{s} \times N_\mathrm{s}$ diagonal matrix with $\bar{\boldsymbol{\lambda}}_l = [\lambda_0^l, \cdots, \lambda_{K-1}^l]^T$, and $\boldsymbol{\omega} = [\boldsymbol{\omega}_{K_\mathrm{p}}^T, \cdots, \boldsymbol{\omega}_{K_\mathrm{p}+K-1}^T]^T$ with $\boldsymbol{\omega}_k = [\omega_{k,N_\mathrm{p}}, \cdots, \omega_{k,N_\mathrm{p}+N-1}]^T$ denotes the colored noise having the covariance matrix $\mathbf{R}_{\boldsymbol{\omega}} = \sigma_0^2\mathbf{G}_0$. Specifically, the first N rows of $\mathbf{\Xi}_{k_\Delta,l}$ are represented as $[\mathbf{0}_{N\times(K_\mathrm{p}+k_\Delta)N}\ \mathbf{A}_{k_\Delta,l}\ \mathbf{0}_{N\times(K-1)N}]$ and each block $\mathbf{A}_{k_\Delta,l}$ is an $N \times N$ circulant matrix with the first row vector of $\big[A_\mathrm{p}((-N_\mathrm{p}+l)\tau T, k_\Delta\nu F), A_\mathrm{p}((-N_\mathrm{p}+l+1)\tau T, k_\Delta\nu F), \cdots, A_\mathrm{p}\big((N_\mathrm{p}+l)\tau T, k_\Delta\nu F\big), \mathbf{0}_{N-2N_\mathrm{p}-1}^T\big]$. Moreover, the condition number of $\mathbf{G}$ is much lower than that of the original equivalent channel matrix for fixed packing factors, which can be verified via numerical analysis. Hence, the received signal model of (3) is expected to considerably mitigate the ill-conditioning problem of MFTN signaling.

According to Theorem 5.8.1 in [22], the block circulant matrices having circulant blocks can be diagonalized by a unitary matrix, i.e., $\mathbf{\Xi}_{k_\Delta,l} = (\mathbf{F}_K \otimes \mathbf{F}_N)^H\mathbf{\Lambda}_{k_\Delta,l}(\mathbf{F}_K \otimes \mathbf{F}_N)$, where $\mathbf{\Lambda}_{k_\Delta,l}$ is an $N_\mathrm{s} \times N_\mathrm{s}$ diagonal matrix. Considering that the product of a unitary matrix $(\mathbf{F}_K \otimes \mathbf{F}_N)$ and a vector can be efficiently obtained by a 2D FFT operation, we reconstruct the received signal model to whiten the colored noise as

$$\begin{aligned}\breve{\mathbf{r}} &= (\mathbf{F}_K \otimes \mathbf{F}_N)\mathbf{r} \\ &= \sum_{l=0}^{L-1} h_l\mathbf{\Lambda}_{0,l}(\mathbf{F}_K \otimes \mathbf{F}_N)\bar{\mathbf{\Lambda}}_l\mathbf{x} + \sum_{k_\Delta\in\mathcal{I}\backslash 0}\mathbf{\Phi}_{k_\Delta}\mathbf{x} + \breve{\boldsymbol{\omega}},\end{aligned} \tag{4}$$

where $\mathbf{\Phi}_{k_\Delta} = \sum_{l=0}^{L-1} h_l(\mathbf{F}_K \otimes \mathbf{F}_N)\mathbf{\Theta}_{k_\Delta}\mathbf{\Xi}_{k_\Delta,l}\bar{\mathbf{\Lambda}}_l$, $\mathbf{\Phi}_0 = \sum_{l=0}^{L-1} h_l\mathbf{\Lambda}_{0,l}(\mathbf{F}_K \otimes \mathbf{F}_N)\bar{\mathbf{\Lambda}}_l$ for $k_\Delta = 0$, $\breve{\boldsymbol{\omega}} = \big(\mathbf{F}_K \otimes \mathbf{F}_N\big)\boldsymbol{\omega}$ is the equivalent AWGN process having the covariance matrix $\mathbf{R}_{\breve{\boldsymbol{\omega}}} \approx \sigma_0^2\big[(\mathbf{F}_K \otimes \mathbf{F}_N)\mathbf{\Xi}_{0,0}(\mathbf{F}_K \otimes \mathbf{F}_N)^H\big] = \sigma_0^2\mathbf{\Lambda}_{0,0}$. When the packing factors are high, the complex-valued diagonal $\mathbf{\Lambda}_{0,0}$ contains lots of entries that are close to zero. To improve the stability of message updating, the covariance matrix of $\breve{\boldsymbol{\omega}}$ is approximated as $\mathbf{R}_{\breve{\boldsymbol{\omega}}} \approx \sigma_{\breve{\omega}}^2\mathbf{I}_{N_\mathrm{s}}$ with $\sigma_{\breve{\omega}}^2 = \frac{\sigma_0^2}{N_\mathrm{s}}\mathbf{1}_{N_\mathrm{s}}^T|\mathbf{\Lambda}_{0,0}|\mathbf{1}_{N_\mathrm{s}}$.

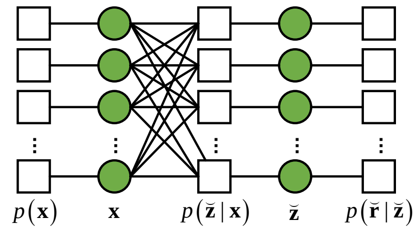

Fig. 2: Factor graph representation of FDE.

III. Iterative Receiver in Multipath Channels

A. GAMP-Based FDE Algorithm

Our goal is to solve the generalized linear mixing problem of estimating a random vector $\mathbf{x}$ from the observation vector $\breve{\mathbf{r}}$ according to the proposed received signal model in (4). According to the factorization of the *a posteriori* probability, i.e., $p(\mathbf{x}|\breve{\mathbf{r}}) \propto \prod_{k,n} p(\breve{r}_{k,n}|\breve{z}_{k,n})p(\breve{z}_{k,n}|\mathbf{x})\prod_{k',n'} p(x_{k',n'})$, we can construct the factor graph containing short dense loops as seen in Fig. 2, where $\breve{\mathbf{z}} = \sum_{k_\Delta\in\mathcal{I}}\mathbf{\Phi}_{k_\Delta}\mathbf{x}$ is the noiseless observation vector and $p(\mathbf{x})$ is the *a priori* probability of $\mathbf{x}$. This results in an excessive computational complexity for typical loopy belief propagation (LBP) message passing algorithm. For efficiently reconstructing the transmitted symbols from the noisy observations in (4), we resort to the GAMP algorithm for decoupling the high-dimensional random linear mixing estimation problem into a series of scalar computations. Based on the central limit theorem and Taylor series expansion, the GAMP algorithm can provide an efficient approximation of the LBP on factor graph, in order to obtain the MMSE solutions [23]. Based on the FD received signal model in (4), we significantly reduce the complexity of the GAMP algorithm. The GAMP-based FDE algorithm proposed for MFTN systems is summarized in **Algorithm** 1.

The pseudo *a priori* messages $\boldsymbol{\nu}^p(i)$ and $\hat{\mathbf{p}}(i)$ updated in Line 3 and 4 of **Algorithm** 1 are the approximations of the messages propagated from the factor nodes $p(\breve{\mathbf{z}}|\mathbf{x})$ to the variable nodes $\breve{\mathbf{z}}$. The messages $\boldsymbol{\nu}^\gamma(i)$ and $\hat{\boldsymbol{\gamma}}(i)$ obtained in Line 7 and 8 update the outgoing messages from the factor nodes $p(\breve{\mathbf{z}}|\mathbf{x})$ to the variable nodes $\mathbf{x}$. By taking the product of both incoming messages at nodes $\mathbf{x}$, we express the *a posteriori* probability of the transmitted symbols as

$$p(\mathbf{x}|\breve{\mathbf{r}}) = \frac{p(\mathbf{x})\mathcal{CN}\big(\mathbf{x}; \hat{\boldsymbol{\gamma}}(i), \mathcal{D}(\boldsymbol{\nu}^\gamma(i))\big)}{\int_{\mathbf{x}} p(\mathbf{x})\mathcal{CN}\big(\mathbf{x}; \hat{\boldsymbol{\gamma}}(i), \mathcal{D}(\boldsymbol{\nu}^\gamma(i))\big)}, \tag{5}$$

where $p(\mathbf{x})$ is the discrete *a priori* probability density function of $\mathbf{x}$, which depends both on the constellation mapping rules and on the *a priori* probabilities of the coded bits. In the turbo receiver, the latter is updated as $p(c_n) = \frac{1}{2}\big[1 + (-1)^{c_n}\tanh\big(\frac{1}{2}L_{\mathrm{dec}}^{\mathrm{e},(i)}(c_n)\big)\big]$, where $L_{\mathrm{dec}}^{\mathrm{e},(i)}(c_n)$ denotes the soft extrinsic information gleaned from the channel decoder. Assuming that each element of $\mathbf{x}$ belongs to the constellation set $\mathcal{S} = \{\mathcal{S}_1, \cdots, \mathcal{S}_M\}$, the *a posteriori* expectation and variance

Algorithm 1 The GAMP-Based FDE Algorithm

1: Initialization: Set $\hat{\mathbf{x}}(1) = \mathbf{0}_{N_\text{s}}$, $\boldsymbol{\nu}^x(1) = \infty$, $\hat{\mathbf{s}}(0) = \mathbf{0}_{N_\text{s}}$.
2: **for** $i = 1$ to I_e **do**
3: $\boldsymbol{\nu}^p(i) = \sum_{k_\Delta \in \mathcal{I}} |\boldsymbol{\Phi}_{k_\Delta}|^2 \boldsymbol{\nu}^x(i)$
4: $\hat{\mathbf{p}}(i) = \sum_{k_\Delta \in \mathcal{I}} \boldsymbol{\Phi}_{k_\Delta} \hat{\mathbf{x}}(i) - \boldsymbol{\nu}^p(i) \odot \hat{\mathbf{s}}(i-1)$
5: $\boldsymbol{\nu}^s(i) = \mathbf{1}_{N_\text{s}} \oslash (\boldsymbol{\nu}^p(i) + \sigma_\omega^2 \mathbf{1}_{N_\text{s}})$
6: $\hat{\mathbf{s}}(i) = (\check{\mathbf{r}} - \hat{\mathbf{p}}(i)) \oslash (\boldsymbol{\nu}^p(i) + \sigma_\omega^2 \mathbf{1}_{N_\text{s}})$
7: $\boldsymbol{\nu}^\gamma(i) = \mathbf{1}_{N_\text{s}} \oslash \left[\sum_{k_\Delta \in \mathcal{I}} |\boldsymbol{\Phi}_{k_\Delta}^H|^2 \boldsymbol{\nu}^s(i)\right]$
8: $\hat{\boldsymbol{\gamma}}(i) = \hat{\mathbf{x}}(i) + \boldsymbol{\nu}^\gamma(i) \odot \left[\sum_{k_\Delta \in \mathcal{I}} \boldsymbol{\Phi}_{k_\Delta}^H \hat{\mathbf{s}}(i)\right]$
9: $\hat{\mathbf{x}}(i+1) = \mathbb{E}\{\mathbf{x} | \hat{\boldsymbol{\gamma}}(i), \mathbf{c}, \boldsymbol{\nu}^\gamma(i)\}$
10: $\boldsymbol{\nu}^x(i+1) = \mathbb{V}\{\mathbf{x} | \hat{\boldsymbol{\gamma}}(i), \mathbf{c}, \boldsymbol{\nu}^\gamma(i)\}$
11: Compute the extrinsic LLRs of the equalizer based on the outgoing messages $\boldsymbol{\nu}^\gamma(i)$ and $\hat{\boldsymbol{\gamma}}(i)$, and then feed them to the channel decoder.
12: Perform BCJR channel decoding and feed the soft extrinsic information to the equalizer.
13: **end for**

of the transmitted symbols in Line 9 and 10 are given by

$$\hat{x}_{k,n}(i+1) \propto \sum_m \mathcal{S}_m p(x_{k,n} = \mathcal{S}_m) \zeta_{k,n}^m(i), \tag{6}$$

$$\nu_{k,n}^x(i+1) \propto \sum_m |\hat{x}_{k,n}(i+1) - \mathcal{S}_m|^2 p(x_{k,n} = \mathcal{S}_m) \zeta_{k,n}^m(i), \tag{7}$$

where $\zeta_{k,n}^m(i) = \exp(-|\mathcal{S}_m - \hat{\gamma}_{k,n}(i)|^2 / \nu_{k,n}^\gamma(i))$.

B. Refined GAMP-Based FDE Algorithm

Since the squared modulus operations increase the condition number of the equivalent channel matrix, the message updates of the proposed GAMP-based FDE algorithm are sensitive to small perturbations. In this section, we introduce average approximations for tackling this problem and then develop a refined GAMP-based FDE algorithm.

We rewrite pseudo *a priori* variance vector $\boldsymbol{\nu}^p(i)$ of the noiseless measurements in Line 3 of **Algorithm** 1 as

$$\begin{aligned}\boldsymbol{\nu}^p(i) &= \sum_{k_\Delta \in \mathcal{I}} \mathcal{D}\big(\boldsymbol{\Phi}_{k_\Delta} \mathcal{D}(\boldsymbol{\nu}^x(i)) \boldsymbol{\Phi}_{k_\Delta}^H\big) \mathbf{1}_{N_\text{s}} \\ &\approx \mathcal{D}\Big[\sum_{l,l'} h_l h_{l'}^* \boldsymbol{\Lambda}_{0,l} \bar{\nu}_{l,l'}^x(i) \mathbf{I}_{N_\text{s}} \boldsymbol{\Lambda}_{0,l'}^H\Big] \mathbf{1}_{N_\text{s}} \\ &\quad + \sum_{k_\Delta \in \mathcal{I} \backslash 0} \mathcal{D}\Big[\sum_{l,l'} h_l h_{l'}^* \bar{\nu}_{l,l'}^x(i) (\mathbf{F}_K \otimes \mathbf{F}_N) \boldsymbol{\Theta}_{k_\Delta} \\ &\qquad \times \varrho_{l,l'}^{k_\Delta}(i) \mathbf{I}_{N_\text{s}} \boldsymbol{\Theta}_{k_\Delta}^H (\mathbf{F}_K \otimes \mathbf{F}_N)^H\Big] \mathbf{1}_{N_\text{s}} \\ &= \sum_{l,l'} h_l h_{l'}^* \bar{\nu}_{l,l'}^x(i) \Big(\boldsymbol{\Lambda}_{0,l} \boldsymbol{\Lambda}_{0,l'}^H \mathbf{1}_{N_\text{s}} + \sum_{k_\Delta \in \mathcal{I} \backslash 0} \varrho_{l,l'}^{k_\Delta} \mathbf{1}_{N_\text{s}}\Big),\end{aligned} \tag{8}$$

where $\bar{\nu}_{l,l'}^x(i) = 1/N_\text{s} \mathbf{1}_{N_\text{s}}^T \bar{\boldsymbol{\Lambda}}_l \mathcal{D}(\boldsymbol{\nu}^x(i)) \bar{\boldsymbol{\Lambda}}_{l'}^H \mathbf{1}_{N_\text{s}}$ and $\varrho_{l,l'}^{k_\Delta} = 1/N_\text{s} \mathbf{1}_{N_\text{s}}^T \boldsymbol{\Lambda}_{k_\Delta,l} \boldsymbol{\Lambda}_{k_\Delta,l'}^H \mathbf{1}_{N_\text{s}}$. Similarly, the outgoing variance vector $\boldsymbol{\nu}^\gamma(i)$ in Line 7 of **Algorithm** 1 is approximated as

$$\begin{aligned}\boldsymbol{\nu}^\gamma(i) &\approx 1 / \sum_{l,l'} h_l h_{l'}^* \Big(\bar{\xi}_{l,l'}^s(i) + \sum_{k_\Delta \in \mathcal{I} \backslash 0} \varrho_{l,l'}^{k_\Delta} \bar{\nu}^s(i)\Big) \mathbf{1}_{N_\text{s}} \\ &= 1/\xi^\gamma(i) \mathbf{1}_{N_\text{s}},\end{aligned} \tag{9}$$

where $\bar{\xi}_{l,l'}^s(i) = 1/N_\text{s} \mathbf{1}_N^T \boldsymbol{\Lambda}_{0,l}^H \mathcal{D}(\boldsymbol{\nu}_k^s(i)) \boldsymbol{\Lambda}_{0,l'} \mathbf{1}_N$, $\bar{\nu}^s(i) = 1/N_\text{s} \mathbf{1}_{N_\text{s}}^T \boldsymbol{\nu}^s(i)$. Moreover, the corresponding outgoing mean vector $\hat{\boldsymbol{\gamma}}(i)$ of the noiseless measurements in Line 8 of **Algorithm** 1 is simplified as

$$\hat{\boldsymbol{\gamma}}(i) = \hat{\mathbf{x}}(i) + \xi^\gamma(i) \sum_{k_\Delta \in \mathcal{I}} \boldsymbol{\Phi}_{k_\Delta}^H \hat{\mathbf{s}}(i). \tag{10}$$

The proposed refined GAMP-based FDE algorithm is summarized in **Algorithm** 2.

Algorithm 2 The Refined GAMP-Based FDE Algorithm

1: Initialization: Set $\hat{\mathbf{x}}(1) = \mathbf{0}_{N_\text{s}}$, $\boldsymbol{\nu}^x(1) = \infty$, $\hat{\mathbf{s}}(0) = \mathbf{0}_{N_\text{s}}$.
2: **for** $i = 1$ to I_e **do**
3: Compute the pseudo *a priori* variance vector of the noiseless measurements $\boldsymbol{\nu}^p(i)$ using (8).
4: Compute $\hat{\mathbf{p}}(i)$, $\boldsymbol{\nu}^s(i)$ and $\hat{\mathbf{s}}(i)$ using Line 4-6 in **Algorithm** 1.
5: Compute the outgoing messages $\boldsymbol{\nu}^\gamma(i)$ and $\hat{\boldsymbol{\gamma}}(i)$ using (9) and (10).
6: Compute $\hat{\mathbf{x}}(i+1)$ and $\boldsymbol{\nu}^x(i+1)$ using Line 9-10 in **Algorithm** 1.
7: Compute the extrinsic LLRs of the equalizer and then feed them to the channel decoder.
8: Perform BCJR channel decoding and feed the soft extrinsic information to the equalizer.
9: **end for**

C. Complexity Analysis

The complexity comparisons of the proposed GAMP-based FDE and the existing equalization algorithms are summarized in TABLE I. The complexity of GMP-based TDE algorithm of [17] is dominated by the inversion of the truncated interference matrix, having a complexity order of $\mathcal{O}[N_\text{s}(2N_\text{I}+1)^2(2K_\text{I}+1)^3]$. The GAMP-based TDE algorithm of [23] has to evaluate N_s^2 complex multiplications for N_s transmitted symbols. The MMSE-based TDE of [24] has a complexity order of $\mathcal{O}(N_\text{s}^3)$ due to the matrix inversion. The complexity of the MMSE-SIC TDE of [14] is entailed the calculation of the MMSE filter coefficients and the complex multiplications of SIC. The former has a complexity order of $\mathcal{O}(L_\text{s}^3)$ owing to the inversion of the truncated ISI interference matrix, where L_s is the length of MMSE filter, while the latter has a complexity order of $\mathcal{O}[(K-1)N]$. For the proposed GAMP-based FDE algorithms, the complexity is dominated by the scalar complex multiplications and the 2D FFT, where the former leads to a complexity order of $\mathcal{O}(N_\text{s})$ and the latter has the complexity $N_\text{s}\log(N_\text{s})$. The calculations of $\check{\mathbf{r}}$, $\hat{\mathbf{p}}(i)$ and $\hat{\boldsymbol{\gamma}}(i)$ require $N_\text{t} = 2K_\text{I}L + 6K_\text{I} + 2L + 2$ N_s-point 2D FFT operations in the GAMP-FDE algorithm, while the calculations of $\boldsymbol{\nu}^p(i)$ and $\boldsymbol{\nu}^\gamma(i)$ has a complexity order of $\mathcal{O}(N_\text{s}^2)$. Moreover, the refined version only requires N_t N_s-point 2D FFTs.

IV. Simulation Results

In this section, we evaluate the BER performance of the proposed FDE algorithms and analyze their convergence properties using extrinsic information transfer (EXIT) charts [25], [26]. We consider a rate-3/4 LDPC code having a length of $N_\text{c} = 4032$ and QPSK modulation. The number of subcarriers

TABLE I: Complexity Analysis

Algorithm	Complexity of the equalizer
GMP-TDE	$\mathcal{O}[N_\text{s}(2N_\text{I}+1)^2(2K_\text{I}+1)^3]$
GAMP-TDE	$\mathcal{O}(N_\text{s}^2)$
MMSE-TDE	$\mathcal{O}(N_\text{s}^3)$
MMSE-SIC-TDE	$\mathcal{O}[(K-1)N]$ + $\mathcal{O}(L_\text{s}^3)$
GAMP-FDE	$\mathcal{O}(N_\text{s}^2)+\mathcal{O}(N_\text{t}N_\text{s}\log N_\text{s})$
Refined GAMP-FDE	$\mathcal{O}(N_\text{t}N_\text{s}\log N_\text{s})$

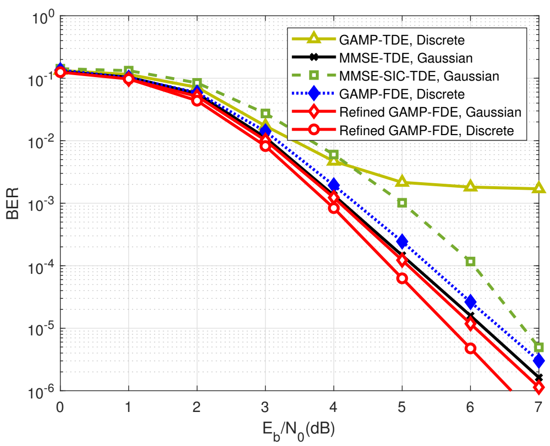

Fig. 3: BER performance of different equalization algorithms for MFTN systems with $\tau=0.9, \nu=0.8$.

is $K=32$ and the number of symbols per subcarrier is $N=256$. The roll-off factor of the RRC shaping pulse is $\beta=0.3$. The number of cyclic postfixes is $K_\text{p}=1$ and $N_\text{p}=12$, where K_I and N_I equal to them, respectively. The fixed truncated lengths can cover the dominant 2D interferences in the following simulations. A multipath channel having $L=8$ taps is considered with the power delay profile $\sigma_{h_l}^2=\exp(-l)/(\sum_l \sigma_{h_l}^2)$. The number of iterations between the equalizer and channel decoder is $I_\text{e}=50$ and the maximum number of LDPC decoding iterations is $I_\text{c}=15$.

In Fig. 3, the BER performance of the proposed GAMP-based FDE algorithms is compared to those of the existing GAMP-TDE of [23] and the MMSE-based TDEs of [14], [24]. The label 'Gaussian' and 'Discrete' refer to the algorithm employing the approximated Gaussian distributions and the exact discrete *a priori* distributions of the transmitted symbols, respectively. Due to the ill-conditioning problem of MFTN signaling, GAMP-TDE fails to converge, hence exhibiting an error floor at BER $=10^{-3}$. Since the MMSE-SIC-TDE employs a truncated interference model for reducing the computational complexity, it inevitably leads to a performance degradation, compared to the MMSE-TDE algorithm. The BER performance of the GAMP-FDE approaches that of the MMSE-TDE, where the former has a significantly lower complexity. Observe that the refined GAMP-FDE algorithm outperforms the MMSE-TDE and an additional $\text{E}_\text{b}/\text{N}_0$ gain can be obtained when we employ the discrete *a priori* probability. This is because the refined GAMP-FDE introduces the average variance vectors for circumventing the problem of having the ill-conditioned matrices in (8) and (9).

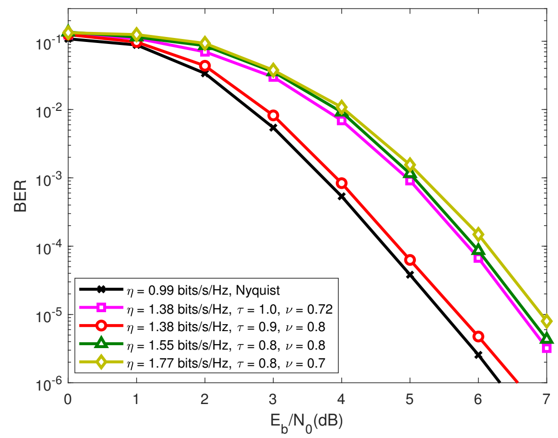

Fig. 4: BER performance of the proposed refined GAMP-FDE algorithm for MFTN systems with various packing factors.

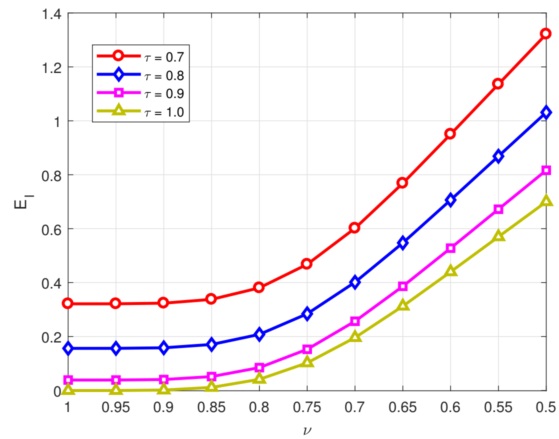

Fig. 5: The energy of the two-dimensional interferences of MFTN signaling employing the RRC pulse with $\beta=0.3$.

The BER performance of the refined GAMP-FDE algorithm proposed for MFTN systems using different packing factors are shown in Fig. 4. Assuming that ς is the cyclic postfix overhead, the SE is calculated as $\eta=\frac{R_c(1-\varsigma)\log_2 M}{\tau\nu(1+\beta)}$ bits/s/Hz [2]. Compared to its Nyquist-signaling counterpart, our MFTN system using $\tau=0.9, \nu=0.8$ attains about 39% higher SE at a negligible BER loss. When we further reduce the packing factors, MFTN signaling can further improve the SE by up to 56% and 79%, respectively, at the cost of 1.2 dB and 1.4 dB $\text{E}_\text{b}/\text{N}_0$ losses at BER $=10^{-5}$. In Fig. 5, we evaluate the interference energy $E_\text{I}=\sum_n\sum_k|A_\text{p}(n\tau T, k\nu F)|^2-|A_\text{p}(0,0)|^2$ of MFTN signaling, where we have $A_\text{p}(0,0)=\int_{-\infty}^{+\infty}|p(t)|^2dt=1$ for a unit-energy shaping pulse. Observe that E_I depends both on the packing factor combinations and on the pulse shaping filter. For a fixed SE, the effects of τ and ν on E_I may be quite different. Here we only discuss MFTN systems employing the classic RRC pulse with $\beta=0.3$. It is seen that MFTN signaling suffers from different E_I for a fixed η. Hence, by jointly optimizing the time and frequency packing factors, we are able to reduce E_I and accordingly improve the BER performance. As shown in Fig. 5, for $\eta=1.38$ bits/s/Hz, MFTN signaling with $\tau=0.9, \nu=0.8$ suffers from a lower E_I, compared to the case of $\tau=1.0, \nu=0.72$. Accordingly,

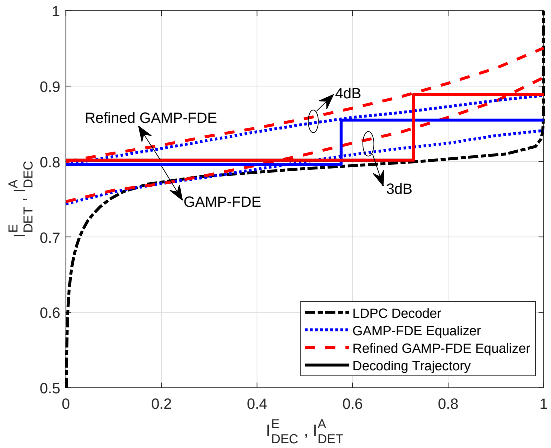

Fig. 6: EXIT chart for the proposed GAMP-FDE algorithms.

the former has 1 dB performance gain at $\mathrm{BER} = 10^{-5}$.

The EXIT curves of the proposed GAMP-based FDE algorithms and that of the rate-$3/4$ LDPC decoder are shown in Fig. 6. There is no open tunnel between the equalizer curve and the decoder curve at $\mathrm{E_b/N_0} = 3$ dB, while an open tunnel emerges at $\mathrm{E_b/N_0} = 4$ dB. The stair-case-shaped decoding trajectories between the equalizer and the channel decoder at $\mathrm{E_b/N_0} = 4$ dB are also included for characterizing the exchange of extrinsic information. It is observed that the proposed GAMP-FDE equalizers require at least 3 iterations between the equalizer and channel decoder for reaching the maximum mutual information point. Moreover, the proposed refined GAMP-FDE equalizer converges faster than the GAMP-FDE, which demonstrates the power of the average approximation employed.

V. Conclusions

In this correspondence, we proposed low-complexity GAMP-based FDE algorithms for MFTN systems operating in multipath channels. To mitigate the ill-conditioning problem of MFTN signaling, we reformulated the received signal model with the aid of a block circulant interference matrix via inserting a few cyclic postfixes. Then, the received signal was transformed to the FD by a 2D FFT to obtain the equivalent white Gaussian noise. Exploiting the GAMP rules, we derived a parametric GAMP-FDE algorithm, which was then further refined based on the average approximations of the variance vectors to circumvent the problems caused by the ill-conditioned matrices. Simulation results showed that MFTN signaling employing the refined GAMP-FDE algorithm significantly improves the transmission rates at a negligible BER degradation, compared to its Nyquist-signaling counterpart.

References

[1] T. Ishihara, S. Sugiura, and L. Hanzo, "The evolution of faster-than-nyquist signaling," *IEEE Access*, vol. 9, pp. 86 535–86 564, Jun. 2021.

[2] P. Banelli, S. Buzzi, G. Colavolpe, A. Modenini, F. Rusek, and A. Ugolini, "Modulation formats and waveforms for 5G networks: Who will be the heir of OFDM?: An overview of alternative modulation schemes for improved spectral efficiency," *IEEE Signal Process. Mag.*, vol. 31, no. 6, pp. 80–93, Nov. 2014.

[3] T. Ishihara and S. Sugiura, "Iterative frequency-domain joint channel estimation and data detection of faster-than-Nyquist signaling," *IEEE Trans. Wireless Commun.*, vol. 16, no. 9, pp. 6221–6231, Sept. 2017.

[4] S. Li, W. Yuan, J. Yuan, B. Bai, D. Wing Kwan Ng, and L. Hanzo, "Time-domain vs. frequency-domain equalization for FTN signaling," *IEEE Trans. Veh. Technol.*, vol. 69, no. 8, pp. 9174–9179, Aug. 2020.

[5] W. Yuan, N. Wu, A. Zhang, X. Huang, Y. Li, and L. Hanzo, "Iterative receiver design for FTN signaling aided sparse code multiple access," *IEEE Trans. Wireless Commun.*, vol. 19, no. 2, pp. 915–928, Feb. 2020.

[6] W. Yuan, N. Wu, Q. Guo, D. W. K. Ng, J. Yuan, and L. Hanzo, "Iterative joint channel estimation, user activity tracking, and data detection for FTN-NOMA systems supporting random access," *IEEE Trans. Commun.*, vol. 68, no. 5, pp. 2963–2977, May 2020.

[7] M. Yuhas, Y. Feng, and J. Bajcsy, "On the capacity of faster-than-Nyquist MIMO transmission with CSI at the receiver," in *Proc. IEEE Globecom Workshops*, Dec. 2015, pp. 1–6.

[8] F. Rusek and J. B. Anderson, "The two dimensional Mazo limit," in *Proc. IEEE Int. Symp. Inf. Theory*, Sept. 2005, pp. 970–974.

[9] M. Jana, L. Lampe, and J. Mitra, "Precoded time-frequency-packed multicarrier faster-than-Nyquist transmission," in *Proc. IEEE 20th Int. Workshop Signal Process. Adv. Wireless Commun.*, Jul. 2019, pp. 1–5.

[10] S. Yang, F. Luo, and L. Yang, "16QAM spectral efficiency frequency division multiplexing transmission with TomlinsonHarashima precoding for intensity modulation and direct detection optical links," *Opt. Quant. Electron.*, vol. 52, no. 9, pp. 1–14, 2020.

[11] L. Bahl, J. Cocke, F. Jelinek, and J. Raviv, "Optimal decoding of linear codes for minimizing symbol error rate," *IEEE Trans. Inf. Theory*, vol. 20, no. 2, pp. 284–287, Mar. 1974.

[12] F. Rusek and J. B. Anderson, "Multistream faster than Nyquist signaling," *IEEE Trans. Commun.*, vol. 57, no. 5, pp. 1329–1340, May 2009.

[13] A. Barbieri, D. Fertonani, and G. Colavolpe, "Time-frequency packing for linear modulations: Spectral efficiency and practical detection schemes," *IEEE Trans. Commun.*, vol. 57, no. 10, pp. 2951–2959, Oct. 2009.

[14] S. Peng, A. Liu, X. Liu, K. Wang, and X. Liang, "MMSE turbo equalization and detection for multicarrier faster-than-Nyquist signaling," *IEEE Trans. Veh. Technol.*, vol. 67, no. 3, pp. 2267–2275, Mar. 2018.

[15] M. Jana, L. Lampe, and J. Mitra, "Interference cancellation for time-frequency packed super-Nyquist WDM systems," *IEEE Photon. Technol. Lett.*, vol. 30, no. 24, pp. 2099–2102, Dec. 2018.

[16] ——, "Design of time-frequency packed WDM superchannel transmission systems," *J. Lightw. Technol.*, vol. 38, no. 24, pp. 6719–6731, Dec. 2020.

[17] Y. Ma, F. Tian, N. Wu, B. Li, and X. Ma, "A low-complexity receiver for multicarrier faster-than-Nyquist signaling over frequency selective channels," *IEEE Commun. Lett.*, vol. 24, no. 1, pp. 81–85, Jan. 2020.

[18] S. Isam and I. Darwazeh, "Simple DSP-IDFT techniques for generating spectrally efficient FDM signals," in *Proc. 7th Int. Symp. Commun. Syst. Netw. Digital Signal Process.*, Jul. 2010, pp. 20–24.

[19] S. B. Makarov, M. Liu, A. S. Ovsyannikova, S. V. Zavjalov, I. I. Lavrenyuk, W. Xue, and J. Qi, "Optimizing the shape of faster-than-Nyquist (FTN) signals with the constraint on energy concentration in the occupied frequency bandwidth," *IEEE Access*, vol. 8, pp. 130 082–130 093, 2020.

[20] A. Rashich and A. Urvantsev, "Pulse-shaped multicarrier signals with nonorthogonal frequency spacing," in *Proc. IEEE Int. Black Sea Conf. Commun. Netw.*, Jun. 2018, pp. 1–5.

[21] A. Gelgor and T. Gelgor, "New pulse shapes for partial response signaling to outperform faster-than-Nyquist signaling," in *Proc. IEEE Int. Conf. Elect. Eng. Photon.*, Oct. 2019, pp. 1–5.

[22] P. J. Davis, *Circulant Matrices*. John Wieley & Sons, Inc, 1979.

[23] S. Rangan, "Generalized approximate message passing for estimation with random linear mixing," in *Proc. IEEE Int. Symp. Inf. Theory*, Jul. 2011, p. 21682172.

[24] M. Tuchler, A. C. Singer, and R. Koetter, "Minimum mean squared error equalization using a priori information," *IEEE Trans. Signal Process.*, vol. 50, no. 3, pp. 673–683, Mar. 2002.

[25] S. ten Brink, "Convergence behavior of iteratively decoded parallel concatenated codes," *IEEE Trans. Commun.*, vol. 49, no. 10, pp. 1727–1737, Oct. 2001.

[26] S. Sugiura and L. Hanzo, "Frequency-domain-equalization-aided iterative detection of faster-than-Nyquist signaling," *IEEE Trans. Veh. Technol.*, vol. 64, no. 5, pp. 2122–2128, May 2015.